USNA --- Trident Scholar project report; no. 285 (2001)

DEVELOPMENT OF AN INVERSE ULTRASONIC RADIATIVE TRANSFER TECHNIQUE

by

Midshipman Kevin D.V. Smith, Class of 2001
United States Naval Academy
Annapolis, Maryland

(signature)

Certification of Advisers' Approval

Associate Professor John A. Burkhardt
Mechanical Engineering Department

(signature)

(date)

Acceptance for the Trident Scholar Committee

Professor Joyce E. Shade
Chair, Trident Scholar Committee

(signature)

(date)

USNA-1531-2

Form SF298 Citation Data

Report Date *("DD MON YYYY")* 07052001	**Report Type** N/A	**Dates Covered (from... to)** *("DD MON YYYY")*

Title and Subtitle Development of an inverse ultrasonic radiative transfer technique	**Contract or Grant Number**
	Program Element Number
Authors Smith, Kevin D. V.	**Project Number**
	Task Number
	Work Unit Number
Performing Organization Name(s) and Address(es) US Naval Academy Annapolis, MD 21402	**Performing Organization Number(s)**
Sponsoring/Monitoring Agency Name(s) and Address(es)	**Monitoring Agency Acronym**
	Monitoring Agency Report Number(s)
Distribution/Availability Statement Approved for public release, distribution unlimited	
Supplementary Notes	
Abstract	
Subject Terms	
Document Classification unclassified	**Classification of SF298** unclassified
Classification of Abstract unclassified	**Limitation of Abstract** unlimited
Number of Pages 39	

REPORT DOCUMENTATION PAGE

Form Approved
OMB No. 074-0188

1. AGENCY USE ONLY (Leave blank)

2. REPORT DATE
7 May 2001

3. REPORT TYPE AND DATE COVERED

4. TITLE AND SUBTITLE
Development of an inverse ultrasonic radiative transfer technique

5. FUNDING NUMBERS

6. AUTHOR(S)
Smith, Kevin D. V.

7. PERFORMING ORGANIZATION NAME(S) AND ADDRESS(ES)

8. PERFORMING ORGANIZATION REPORT NUMBER

9. SPONSORING/MONITORING AGENCY NAME(S) AND ADDRESS(ES)
US Naval Academy
Annapolis, MD 21402

10. SPONSORING/MONITORING AGENCY REPORT NUMBER
Trident Scholar project report no. 285 (2001)

11. SUPPLEMENTARY NOTES

12a. DISTRIBUTION/AVAILABILITY STATEMENT
This document has been approved for public release; its distribution is UNLIMITED.

12b. DISTRIBUTION CODE

13. ABSTRACT:
The focus of this research is the development of an inverse ultrasonic radiatve transfer technique for materials characterization. The technique characterizes multiple scattering materials by estimating the way a typical scatterer redirects ultrasonic intensity into new directions. The way in which a scatterer redistributes ultrasonic intensity is described by the shape of its phase function. The developed technique relies on the gathering of backscattered ultrasonic intensity for the purpose of determining the Legendre coefficients of the phase function. This determination is achieved through an approximate inverse solution of the radiative transfer equation (RTE).

14. SUBJECT TERMS
inverse ultrasonic radiative transfer technique; materials characterization

15. NUMBER OF PAGES
39

16. PRICE CODE

17. SECURITY CLASSIFICATION OF REPORT	18. SECURITY CLASSIFICATION OF THIS PAGE	19. SECURITY CLASSIFICATION OF ABSTRACT	20. LIMITATION OF ABSTRACT

1.0 INTRODUCTION

The focus of this research is the development of an inverse ultrasonic radiative transfer technique for materials characterization. The technique characterizes multiple scattering materials by estimating the way a typical scatterer redirects ultrasonic intensity into new directions. The way in which a scatterer redistributes ultrasonic intensity is described by the shape of its phase function. The developed technique relies on the gathering of backscattered ultrasonic intensity for the purpose of determining the Legendre coefficients of the phase function. This determination is achieved through an approximate inverse solution of the radiative transfer equation (RTE).

For its application in this research, the RTE is simplified to the scalar plane-parallel radiative transfer equation. Ultrasonic transducers are used to simulate a plane wave through a superposition of spherical sources. An experiment was then designed that exploited these simplifications. A source transducer was scanned over the face of an acoustic phantom to simulate the plane wave while the receiver measured backscattered intensity at twelve equally spaced azimuthal angles around the specimen. The phantoms employed in the experiment were composed of biomedical grade agarose with a suspension of glass beads. The total backscattered intensity from all directions was then used in the diffusion approximation to solve for the Legendre coefficients.

1.1. ULTRASONIC TESTING AND IMAGING

Ultrasonic testing is one of several nondestructive techniques available for the characterization of materials and for the detection and characterization of flaws. The

information obtained from ultrasonic NDT is usually based on propagation velocity in the material. Propagation velocity can be determined from the time it takes an ultrasonic pulse to traverse through a material and the thickness of the material. It is more common, though, to measure material thickness using a known propagation velocity and a time of flight measurement for the ultrasonic pulse. This allows for the detection of corrosion or flaws within the material if the measured thickness is smaller than the expected thickness. A procedure for testing welds has also been developed which uses information obtained from moving the ultrasonic probe over multiple locations on the weld. Ultrasonics can also be used to measure stress, detect leaks in pressure vessels, detect hydrogen attack, measure ID oxide scale in boiler tubes, detect cracks in turbines, bolt inspection, and numerous other applications (Nondestructive testing handbook, 1982).

1.2. LIMITATIONS OF ULTRASONIC TESTING AND IMAGING

While ultrasonic NDT and imaging has been employed successfully for systems with relatively simple or no microstructures, current methods fail when attempting to characterize materials with complex microstructures. This is because the models are based on the idea of coherent propagation. In coherent ultrasonics the input signal enters the material with a known shape. If it encounters a flaw as it traverses the material, this is evident in the shape of the received signal (figure 1).

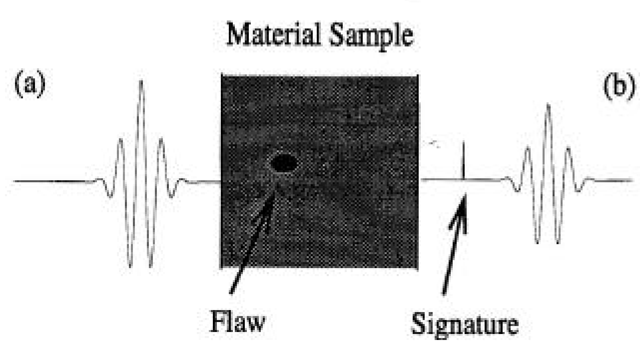

Figure 1. Coherent Ultrasonic Propagation: (a) ultrasonic input signal, (b) ultrasonic receiver signal.

Unfortunately, coherent techniques fail for many systems of vital importance due to the inherent inhomogeneity and complexity of their microstructures. In many materials, as the signal propagates, it is scattered many times, creating a diffuse or

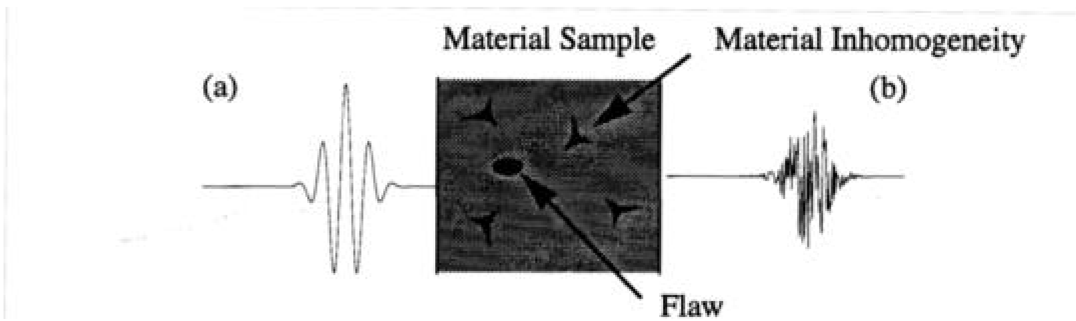

Figure 2. Diffuse Ultrasonic Propagation: (a) ultrasonic input signal, (b) ultrasonic receiver signal.

incoherent output signal (figure 2). During the traversal, it is not only the flaw that changes the signal, but also the structure of the material itself. This makes it virtually impossible to distinguish between the change in the signal caused by a flaw and that caused by the structure of the material itself. This is because the multiple scattering characteristics of the material's microstructure were not modeled in coherent ultrasonics and therefore could not be accounted for. Some examples of materials with complex multiple scattering microstructures include wood, polycrystals, and many human tissues.

To understand better the difference between complex and simple microstructures, a closer examination of how the presence of scatterers in a material affects the propagation of an acoustic signal is useful. When no

Figure 3. Coherent propagation Example

scatterers are present, an acoustic signal is largely unaffected by the material when it propagates from a transmitter to a receiver (figure 3). When the scatterer density of a material is sparse, then a single scattering approximation can be made. This assumes that the signal experiences a single scattering event as it traverses the material sample. The portion of the wave that has been doubly or multiply scattered is assumed to be negligible.

As the scatterer density of the material increases, then the single scattering approximation is no longer valid. The signal arriving at the receiver no longer resembles the source signal due to its interaction with the scattering medium. The character of the source signal has been attenuated by scattering and absorbed along the scattering path, and the scattered rays have likewise been attenuated in the same manner due to multiple scattering (figure 4). Ultimately, what is needed to successfully employ ultrasonics in materials with complex microstructures is a propagation model that takes multiple scattering into account. Such system models for electromagnetic systems do currently exist, and are currently in use in many forms of remote sensing.

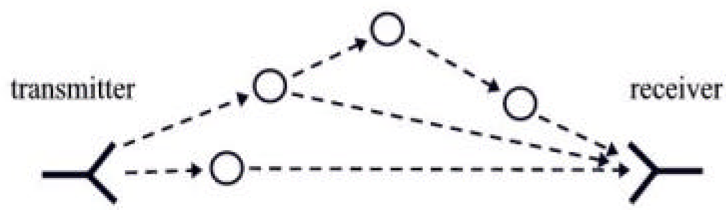

Figure 4. Multiple Scattering Example

1.3. REMOTE SENSING AND NONDESTRUCTIVE TESTING

Remote sensing, like nondestructive testing, deals with the ability to characterize something from outside of that system. An example is Doppler radar, where waves sent into a storm system are scattered by many things such as rain, snow, or even bugs and dust.

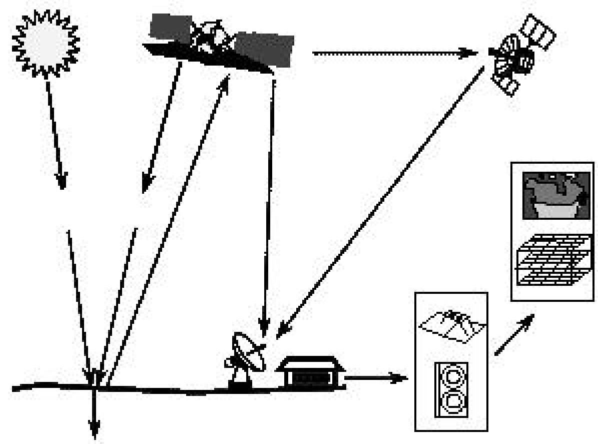

Figure 5. Remote Sensing Example

Some of this scattered wave energy is reflected back to the antenna, where it is analyzed to determine the location and intensity of precipitation. While Doppler radar is based on single scattering theory, there are also presently many models employed in remote sensing applications that allow the use of electromagnetic waves to characterize complex multiple scattering systems. NASA uses remote sensing to determine characteristics of the earth's surface from satellites in space. A satellite in orbit around the earth pulses a signal at the ground (figure 5). The backscattered signal is a combination of directly reflected energy, and energy that has been scattered many times due to things such as vegetation, structures, and terrain. From this backscattered signal, NASA is able to characterize things such as vegetation type and land use for a specific area. The key to bridging the gap between applying electromagnetic and ultrasonic waves in nondestructive testing applications is the existence of an ultrasonic propagation model that takes multiple scattering into account. A multiple scattering model for ultrasonics

termed the ultrasonic radiative transfer equation was recently developed (Weaver, 1990, Turner, 1994).

2.0 DIFFUSE ULTRASONIC BACKSCATTER THEORY

For materials with relatively few scatterers, it is possible to describe the propagation characteristics of waves using single scattering approximations or first order multiple scattering (Ishimaru, 1978). When the scatterers in a material become more numerous, the wave intensity becomes more incoherent and single scattering or first order multiple scattering can no longer characterize the wave. There are two theories that have been used to overcome these limitations: analytical theory and transport theory.

Analytical theory seeks to characterize all multiple scattering, diffraction, and interference effects mathematically. The calculations using this method become so difficult that the best solutions are only approximations valid for a specified range of values. Transport theory, or radiative transfer theory, focuses directly on the transport of energy through a particulate medium. The basic differential equation of transfer, known as the radiative transfer equation, is flexible and capable of modeling many physical phenomena. Recently, an ultrasonic version of the radiative transfer equation has been developed (Weaver, 1990, Turner, 1994). With the derivation of the ultrasonic radiative transfer equation, it became possible to apply transport theory in ultrasonic applications.

In its most general form the ultrasonic radiative transfer equation (URTE) is a vector valued integro-differential equation describing the propagation of multiply scattered wave energy in a randomly disordered medium supporting several wave types. As a result of the complexity of the URTE, it is necessary both to make some

simplifications to facilitate production in the laboratory of the modeled phenomenon, and to simplify the mathematical solution. For this research, the scattering characteristics of the material are assumed to be uniform. The vector values of intensity are all combined into a single scalar intensity. These assumptions yield a single scalar intensity field, $I(z,m,f,t)$, only dependent on the depth into the material, z, polar angle, è, typically expressed by its direction cosine, $m = \cos(q)$, the azimuthal angle, f, and time, t.

2.1. THE SCALAR RADIATIVE TRANSFER EQUATION

While the radiative transfer equation can be derived rigorously by ensemble averaging the wave equation (Barabanenkov, 1968, Weaver, 1990), a great deal of understanding about the RTE and its parameters can be gained through a heuristic derivation of the RTE (Ishimaru, 1978). Following Ishimaru, consider a small volume taken from a multiply scattering material, shown in figure 6 (Ishimaru, 1978). The element has cross section *da* and element length *ds*. Define ç as the number of scatterers per unit volume, yielding $hdads$ scatterers in the volume considered.

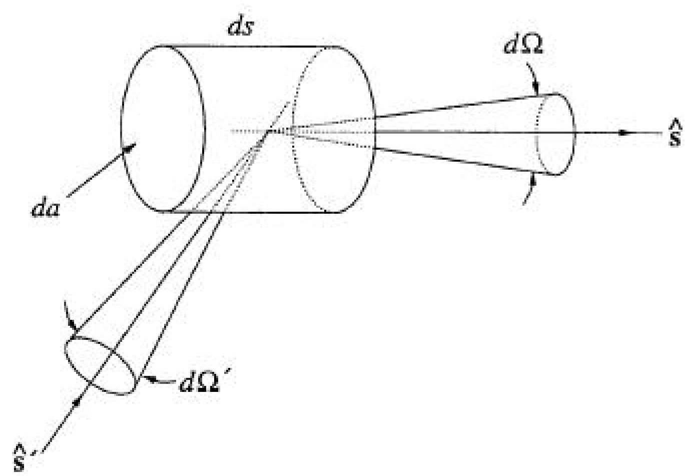

Figure 6. Propagation through the scattering volume in the direction and emission into the ´ direction.

Interest lies in predicting the specific intensity observed in the direction defined by the unit vector . *Specific intensity,* $I(\mathbf{r},t,\hat{\mathbf{s}})$, is defined as the energy per unit area, per unit time, through a differential area, d**a** and within a differential solid angle, dÙ, in the direction of a unit vector **.** More simply, specific intensity is the power flux within differential of solid angle, dÙ, in the direction . It has the units of W m^{-2} sr^{-1} Hz^{-1}. The more common quantity, intensity, is defined as the amount of radiant energy per unit area per unit time and equals the total specific intensity over all solid angles.

The energy emergent from the volume in the direction is then *I*(s,t)*dadtd*Ù. Since the energy moves at a speed of c, the energy a time dt=ds/c later in the direction is *I*(s+ds,t+dt)*dadtd*Ù. As the energy moves along the scattering path, there is a loss attributed to scattering and absorption in the material. There is also a gain in energy due to reemission from other directions into the direction of interest. This gain and loss of energy can be written as an energy balance for the elemental volume, given by

$$I(s+ds,t+dt)dadtd\Omega - I(s,t)dadtd\Omega = -sI(s,t)dadsdtd\Omega + he(s,t)dadsdtd\Omega . \qquad (1)$$

In equation (1), $s = hg^a + hg^s$ is defined as the total attenuation, with g^a defined as the absorption cross section per scatterer, g^s is the scattering cross section per scatterer, and $e(s,t)$ is the emission coefficient per scatterer. The absorption cross section accounts for both absorption of energy by interaction with a scatterer, as well as dissipation of energy in the medium. Likewise, the emission coefficient accounts for emission due to scattering events and from energy sources within the medium. It is implied by equation (1) that

$$\frac{\partial I(s,t)}{\partial s}ds + \frac{\partial I(s,t)}{\partial t}dt = -sI(s,t)ds + he(s,t)ds. \tag{2}$$

Since ds=cdt, Equation (2) becomes

$$\frac{\partial I(s,t)}{\partial s} + \frac{1}{c}\frac{\partial I(s,t)}{\partial t} = -sI(s,t) + he(s,t). \tag{3}$$

In three dimensions, the radiative transfer equation becomes

$$\nabla \bullet \hat{\mathbf{s}} I(\mathbf{r},t,\hat{\mathbf{s}}) + \frac{1}{c}\frac{\partial I(r,t,\hat{\mathbf{s}})}{\partial t} = -sI(\mathbf{r},t,\hat{\mathbf{s}}) + he(\mathbf{r},t,\hat{\mathbf{s}}), \tag{4}$$

where $\hat{\mathbf{s}}$ is the propagation direction, $\mathbf{r}$ is the space vector and the total attenuation has been assumed to be independent of $\hat{\mathbf{s}}$.

It now remains to describe the emission contribution, ε, in terms of the scattering characteristics of the medium. This can be accomplished by realizing that the intensity reemitted into the $\hat{\mathbf{s}}$ direction is composed strictly of intensity scattered into the $\hat{\mathbf{s}}$ direction from other directions. With that in mind, consider the volume in Figure 6, with incident intensity propagating into the scattering volume from the $\hat{\mathbf{s}}'$ direction and scattering into the $\hat{\mathbf{s}}$ direction. Upon scattering, the incident intensity from the $\hat{\mathbf{s}}'$ direction will be redistributed into all propagation directions. Our interest is in the proportion of the

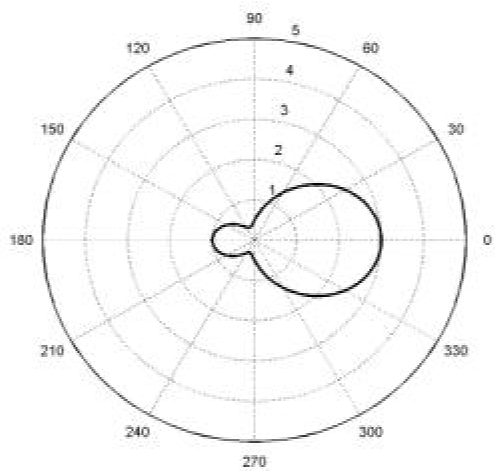

Figure 7. Phase function.

incident intensity scattered into the $\hat{\mathbf{s}}$ direction. This information is characterized by a scattererer's phase function, which describes the angular distribution of scattered intensity. Figure 7 shows a sample phase function for an incident intensity traveling at 0 , or rightward. The distance of the curve from the origin represents the proportion of intensity expected to scatter in that direction. For example, for the phase function shown a great deal more intensity is expected to be scattered forward (0) than backward (180).

In general terms, the phase function describes the intensity scattered from the $\hat{\mathbf{s}}'$ direction into the $\hat{\mathbf{s}}$ direction, and is defined by $q(\hat{\mathbf{s}},\hat{\mathbf{s}}')\frac{d\Omega}{4p}$. The phase function is normalized so that

$$\frac{1}{4p}\int_{\Omega=4p} q(\hat{\mathbf{s}},\hat{\mathbf{s}}')\,d\Omega = g^{s}, \tag{5}$$

where g^{s} is the scattering cross section. If scattering is isotropic, or independent of the direction of propagation and reception, then

$$q(\hat{\mathbf{s}},\hat{\mathbf{s}}') = g^{s}. \tag{6}$$

We can now calculate the intensity reemitted into the $\hat{\mathbf{s}}$ direction from all other propagation directions by integrating the phase function over all solid angles yielding the emission coefficient, ε,

$$e(\mathbf{r},t,\hat{\mathbf{s}}) = \frac{1}{4p}\int q(\hat{\mathbf{s}},\hat{\mathbf{s}}')\,\boldsymbol{I}(\mathbf{r},t,\hat{\mathbf{s}})\,d\Omega'. \tag{7}$$

The full RTE is then written

$$\nabla \bullet \hat{\mathbf{s}}\,\boldsymbol{I}(\mathbf{r},t,\hat{\mathbf{s}}) + \frac{\partial \boldsymbol{I}(r,t,\hat{\mathbf{s}})}{\partial t} + c\,s\,\boldsymbol{I}(\mathbf{r},t,\hat{\mathbf{s}}) = \frac{c}{4p}\int p(\hat{\mathbf{s}},\hat{\mathbf{s}}')\,\boldsymbol{I}(\mathbf{r},t,\hat{\mathbf{s}})\,d\Omega', \tag{8}$$

where $p = hq$.

While the RTE, equation 8, is capable of modeling very complex multiply scattering materials, it is necessary to make some simplifications to facilitate the mathematical solution. With

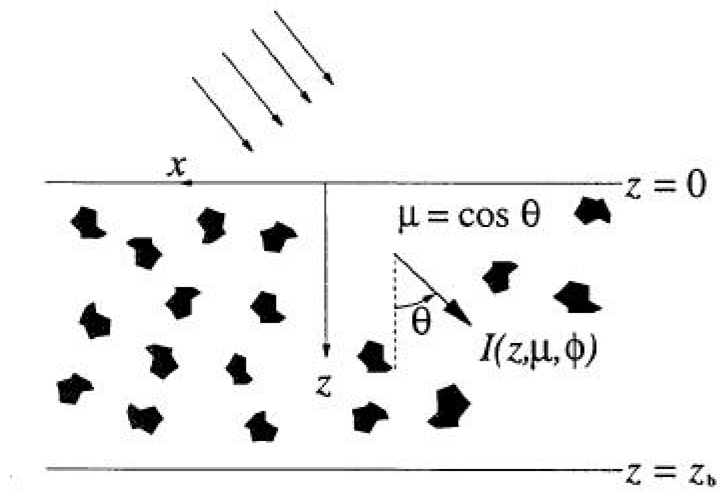

Figure 8. Geometry of a plane-parallel medium.

this objective, the geometry of the scattering sample will be simplified by considering a multiple scattering half-space illuminated by an infinite plane wave propagating in the direction m_o (figure 8). The characteristics of the material are assumed to be independent of position (Chandrashekar, 1960). These assumptions yield a single scalar intensity field, I$(z,ì,j)$, only dependent on the depth into the material, z, polar angle, è, typically redefined by its direction cosine, ì = cos (è), and azimuthal angle, j, measured in a right-hand sense from the x-axis. With these assumptions one gets what is termed the plane-parallel RTE, shown in its normalized form,

$$m\frac{\partial I(z,m,f,t)}{\partial z} + \frac{\partial I(z,m,f,t)}{\partial t} + I(z,m,f,t) = \frac{1}{4p}\int_0^{2p}\int_{-1}^{1} p(m,f,t;m',f')I(z,m',f',t)\,dm'df'. \quad (9)$$

The first term, $m\frac{\partial I(z,m,J,t)}{\partial z}$, accounts for the change in intensity of the wave with change in depth, or in the z-direction. The second term, $sI(z,m,j,t)$, accounts for the loss in intensity by scattering and absorption. The third term,

$\frac{1}{4p}\int_0^{2p}\int_{-1}^{1} p(m, f, t; m', f') I(z, m', f', t) dm' df'$, represents all the intensity reemitted from all directions into the direction of interest, $\hat{\mathbf{s}}$.

The RTE provides many parameters that could possibly be exploited to characterize a material. The most obvious choices are the total intensity attenuation, ó, which is compromised of two components, $ã^{a}$ and $ã^{s}$, and the phase function, $p(z, m, m')$ because they carry the most information. The problem with using either the scattering or absorption parameters to characterize a material is that for different materials, these parameters can have the same value. Instead, the phase function is characterized because it describes the shape of the backscattered intensity in all directions, and is a parameter that is unique to a material.

2.1.1. LEGENDRE POLYNOMIAL EXPANSION OF THE PHASE FUNCTION

Characterization of a scattering medium by its phase function requires that the phase function itself be characterized. This is most commonly accomplished by representing the phase function in terms of a series of Legendre polynomials of the form (Chandreshakar, 1960, Ishimaru, 1978),

$$p(\cos\Theta) = \sum_{l=0}^{\infty} \boldsymbol{v}_l P_l(\cos\Theta) . \tag{10}$$

Legendre polynomials are orthogonal like sines and cosines.

$$\int_{-1}^{1} P_m(x) P_n(x) dx = \boldsymbol{d}_{nm} \tag{11}$$

Expanding the phase function in a Legendre polynomial series yields an infinite list of coefficients, w_l, which characterize the material (figure 9). The Legendre coefficients give weight to the contribution that each Legendre polynomial has in characterizing the shape of the phase function. The zeroth Legendre polynomial, for example, describes the average value of the phase function over all scattering angles.

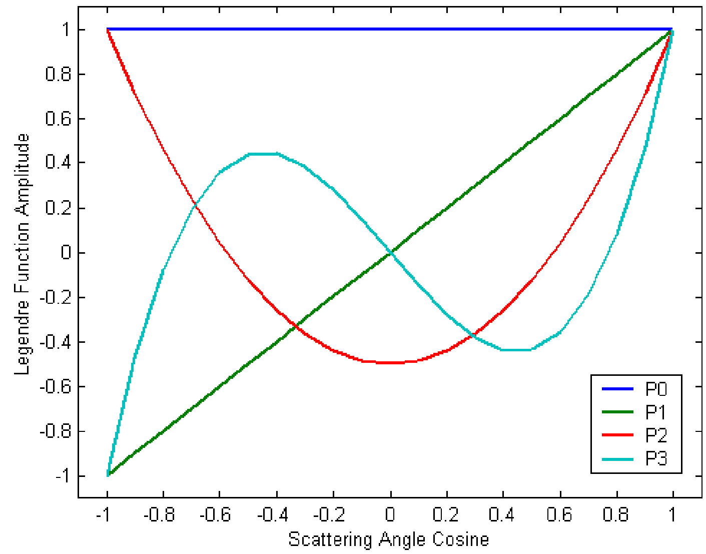

Figure 9. Graph of first four Legendre polynomials

2.2. DIFFUSE BACKSCATTER APPROXIMATION

No known solution of the radiative transfer equation, equation 8, is available for a general phase function (Chandrashekar, 1960). Consequently, numerous simplifications are made to the RTE to allow its analytical solution. One common simplification has already been employed: that is the consideration of a plane parallel geometry. Other useful simplifications include restriction to isotropic scattering (Chandrashekar, 1960). Isotropic scattering, by definition, is constant with scattering angle yielding only one nonzero Legendre polynomial coefficient, thus, limiting its potential for material characterization. The approach employed in this study will involve a diffusion equation approximation to the RTE (Ishimaru , 1978, Weaver, 1990, Turner, 1994).

The derivation of the diffusion approximation to the RTE and its solution for backscatter intensity has already been performed by McCormick and will be summarized in the following paragraphs (McCormick, 1982). The details of the technique and methods are, however, beyond the scope of this project and are left for the interested reader to explore.

The essential element of the technique, for the purpose of this study, is to expand simultaneously the specific intensity in a Fourier azimuthal cosine series,

$$I(z,m,\boldsymbol{j}) = \sum_{m=0}^{\infty} I^{m}(z,m)\cos(m\boldsymbol{j}) \tag{12}$$

and the phase function in a Legendre polynomial series,

$$p(\cos\Theta) = \sum_{l=0}^{\infty} \boldsymbol{v}_l P_l(\cos\Theta)\,. \tag{13}$$

These and other mathematical techniques allow for the derivation of a diffusion equation governing the energy density of the mth Fourier coefficient, E^m, in the sample as a function of position and time,

$$\frac{\partial E^m}{\partial t} = D^m \frac{\partial^2 E^m}{\partial z^2}, \tag{14}$$

where D^m is the mth order diffusion coefficient,

$$D^m = \frac{c}{\left[\left(\frac{2m+3}{2m+1}\right)\boldsymbol{v}_m - \boldsymbol{v}_{m+1}\right]}. \tag{15}$$

Applying the proper boundary conditions then allowed McCormick to calculate an expression for the mth Fourier component of the backscattered intensity from both a finite slab,

$$I^{m}(z,m;t)=K_{1}e^{-\left(1-\frac{\nu_{m}}{2m+1}\right)ct} \tag{16}$$

and a semi-infinite half-space,

$$I^{m}(z,m;t)=K_{2}t^{-3/2}e^{-\left(1-\frac{\nu_{m}}{2m+1}\right)ct}, \tag{17}$$

where both K_1 and K_2 are unimportant constants for the purpose of determining ν_m. K_1 and K_2 are of no interest because they only provide a scaling effect. They play no role in the characterization of the shape. The Legendre weighting factor is the sole parameter that describes the shape. It determines the contribution of each Legendre polynomial to the overall characterization of the phase function.

3.0 THE EXPERIMENTAL METHOD

In the previous section, an approximate expression was derived for the backscattered intensity from a multiply scattering medium based on a diffusion approximation. The translation of the mathematics into a tangible and feasible experimental method and setup is imperative to the success of characterizing the material. Such a setup is not trivial. While an infinite plane wave greatly simplifies calculations on paper, recreating it in the laboratory is not easy. In addition, an experimental apparatus must be designed that can measure the intensity data so that the Legendre coefficients can be deduced from the backscattered intensity measurements. This introduces the need to measure the intensities at discrete azimuthal angles.

3.1. PLANE WAVE APPROXIMATION AND TRANSDUCER SELECTION

As has been stated, the creation of infinite plane waves in the laboratory is not trivial; it is in fact impossible. One can, at best, approximate an infinite plane wave. Directional transducers provide a simple and inexpensive way to generate an ultrasonic pulse. In the far field all directional transducers can be modeled as spherical sources. Due to the cost of multiple directional transducers, as well as the convenience of using only one transducer, it was decided that one source and one receiver transducer would be used. Two ways were examined to approximate infinite plane wave excitations in the laboratory: one involving manipulation of the transducer beam size, and one achieved through scanning a single transducer. In both cases, Panametrics high frequency immersion transducers were considered as they are readily available on the market, relatively cheap, and easy to use and integrate into the apparatus.

Figure 10. Various Panametrics Ultrasonic Transducers.

The first technique considered the size of the ultrasonic beam emitted by the transducer. At a given frequency, a transducer can be purchased in a variety of diameters (figure 10). The diameter of the element at a given frequency determines the beam diameter according to the equation

$$BeamDiameter(-6dB) = \frac{1.02Fc}{fD}, \tag{18}$$

where F is the focal length of the transducer, c is the material sound velocity, f is the transducer frequency, and D is the element diameter. The diameter of the beam is determined to be where the intensity is 6 dB less than that at the center. The beam diameter represents the size of the spot illuminated with acoustic energy. In order for the infinite plane wave approximation to be valid, the beam diameter of the source needed to be larger by at least an order of magnitude than the beam diameter of the receiver. If the source has a much larger beam diameter than the receiver, then the plane wave that the receiver detects can be approximated to be infinite. The beam diameters for transducers from frequencies of 0.5 to 10 megahertz were calculated. These results can be seen in Appendix (1). The beam diameter at a given frequency did not change significantly, so it was determined that this method of approximating an infinite plane wave would not be feasible.

3.1.1. PLANE WAVE SIMULATION: SUPERPOSITION

An alternative for simulating an infinite plane wave is achieved through the scheme by which you pulse and receive multiple times for a single plane wave. If you focus the receiver at a set point on the specimen and then receive while traversing the source over the entire face of the specimen, then a plane wave can be simulated through the superposition of spatially distributed spherical sources (figure 11). This method of infinite plane wave simulation is independent of the transducer selection, but instead plays a significant role in the design of the apparatus for the experiment.

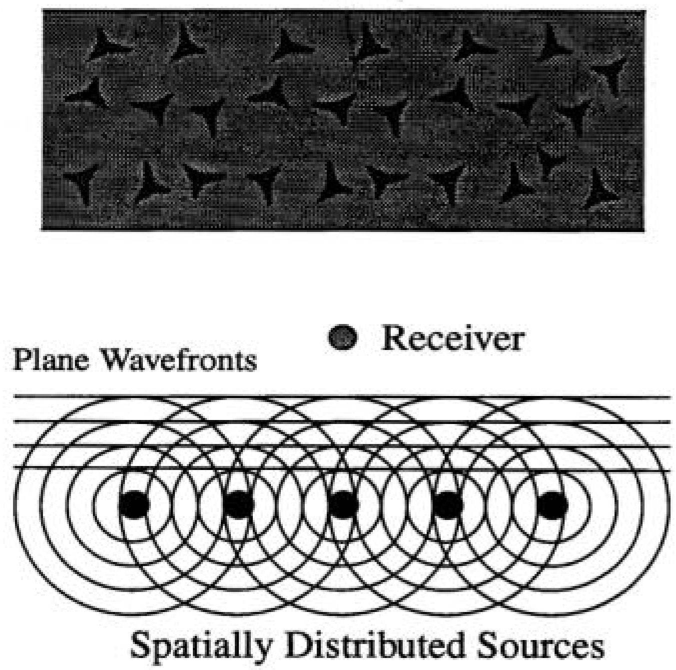

Figure 11. Experimental Configuration for Plane Wave Source

3.2. INTENSITY MEASUREMENT: AZIMUTHAL POSITIONING

In order to evaluate the Fourier azimuthal cosine decomposition (equation 12), the backscattered intensity as a function of azimuthal angle must be known. This introduces the need to measure the intensities at discrete azimuthal angles.

3.3. EXPERIMENTAL APPARATUS

To implement the scanning scheme dcescribed in section 3.1.1 for the simulation of an infinite plane wave, it was necessary to design an original apparatus. The apparatus was designed to be used in conjunction with a Sonix C-Scan system. This scanner is capable of moving the source over the face of the specimen. The apparatus had to be designed to position the receiver at various azimuthal angles around the specimen. It was also necessary that the apparatus be adjustable in order to position the receiver at the optimum focal length. The apparatus was constructed both from products available on the market and with original pieces constructed in the Naval Academy machine and project shop.

The Sonix C-Scan system provides five degrees of freedom in positioning the transducer (figure 12). The apparatus interfaces to a computer that provides complete control and automation of the movement. The computer can also take in and analyze data from the transducer. The movement of the transducer is achieved through a system of servo motors controlled by software provided with the scanner. These motors are capable of very fine positioning. The entire positioning system is attached to a large water tank, since most ultrasonic

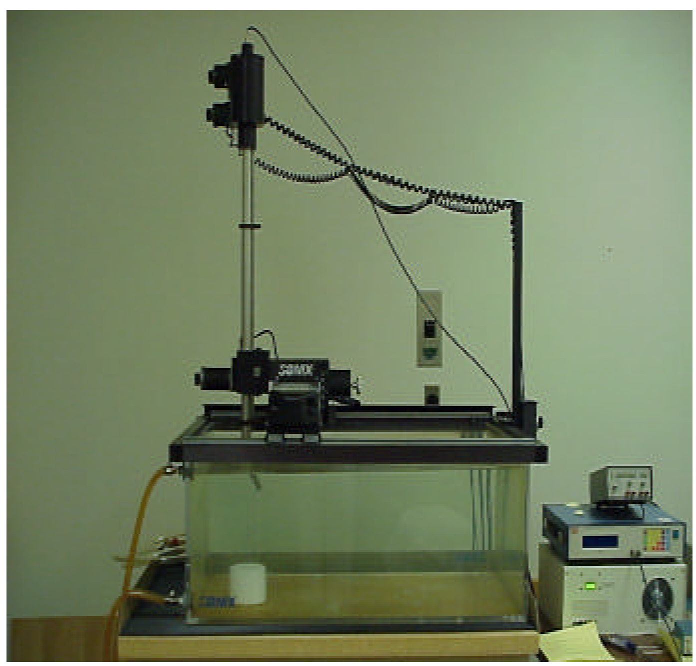

Figure 12. Sonix C-Scan system.

testing is done underwater. The software is provided to move the scanner in a variety of scan patterns.

A C-Scan scheme moves the transducer through a square raster pattern. One first moves the transducer to the desired start position. In the software, it is then possible to define the size of the box to be scanned and the size of the step in both the x and y directions. For a C-Scan you are able to automate the movement in two selected degrees of freedom. Once the size of the box and the step resolution are entered, the scan begins and the C-Scan system moves the transducer in the desired pattern through the defined space in the tank.

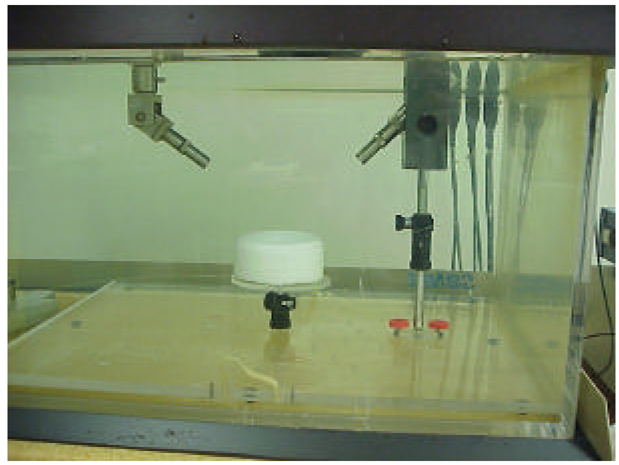

Figure 13. Experimental Setup.

In order to design the apparatus, information about the focusing characteristics of the transducers needed to be determined. Using the documentation provided by Panametrics on their ultrasonic transducers, the necessary focal length for each was ascertained. This formed the basis for the design of the experimental apparatus (figure 13). The movement of the source is automated through the C-

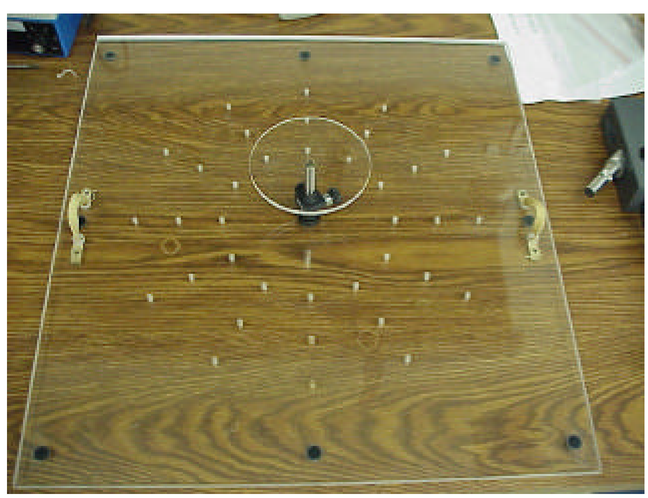

Figure 14. Lucite base with holes drilled for positiong.

Scan system, so the designed apparatus was for the positioning of the receiver. It was determined that two radii, one at 7” and one at 10”, would give the proper distance from the center of the specimen for focusing at the desired polar angles of 30°, 45°, and 60°. The experimental phantom would be located at the center of these two radii, on an adjustable height specimen table. On a large piece of Lucite, twelve sets of holes were drilled on each radius at 30° intervals, with the midpoint between each set of holes being on the radius line (figure 14). One was also drilled at the center of the radii. This allowed for the necessary azimuthal positioning around the specimen to take the backscattered intensity measurements.

Adjustable posts and steel positioning rods, both purchased from the market governed the height of both the specimen table and the receiver. These screwed directly into the holes drilled in the Lucite. The desired polar angle orientation for the receiver was achieved through a plastic block, in which three holes were drilled corresponding to the three determined polar angles. This plastic block screwed to the top of the adjustable posts. In each hole fit a search tube, which held the transducer and allowed the distance from the specimen to be adjusted for focusing (figure 15). The specimen sat on a round Lucite plate that affixed to the top of the positioning post (figures 13, 14).

Figure 15. Receiver positioning apparatus.

3.4. ULTRASONIC PHANTOMS

For performance of the backscatter experiments a material sample is required with known and, ideally, controllable scattering characteristics. Several material systems were considered including custom cast brasses, aluminum foams (figure 16), and agarose based "phantoms." Agarose based phantoms were chosen because they have highly controlled scattering characteristics and are supported by a large foundation of literature from the medical ultrasonics community.

The ultrasonic phantoms constructed for this experiment were made using SeaKem® LE agarose from the FMC corporation. This is a molecular biology grade agarose, commonly used for electrophoresis. Agar is a gelatin-like substance made primarily from two types of red seaweed: Gelidium and Gracilaria. Agar is insoluble in cold water but readily dissolves in water at ~90°F. The scatterers employed in the phantoms were Potters Sphericel® hollow glass beads. These beads are chemically inert and nonporous. They were chosen due to their density of 1.1 g/cc, which is almost the same as that of water. It was desirable that the beads be neutrally buoyant in water so that once they were added to the agarose liquid, they would remain suspended and randomly distributed throughout the phantom as it solidified.

Figure 16. Duocel® Aluminum Foam Samples

3.4.1. PHANTOM SELECTION AND COMPOSITION

Many options were available as candidates to be used as ultrasonic phantoms in the experiment. The first such candidate was an aluminum matrix that is available on the market. This specimen could not be used, though, because the matrix was too random to be modeled mathematically. The two other alternatives were both agarose specimens; one was readily available on the market and the other could be created on site.

The prefabricated phantom specimens come with a known bead distribution. What presented problems were that these phantoms were encased in a plastic covering to maintain integrity. It was thought that this covering would create problems with the received signal, because it cannot easily be matched with derived backscatter theory. The prefabricated phantoms were also a bit expensive and, as a result, were not tested for the experiment.

It was determined that a phantom constructed on premises would best serve the needs of the experiment. Such phantoms were relatively easy and quick to create. The most significant problem that had to be overcome was getting a uniform glass bead distribution in the specimen while allowing it to cool. This problem was overcome by the use of neutrally buoyant glass beads sold on the market and commonly used in flow visualization experiments in fluids mechanics experiments. Although these beads were smaller than desired, obtaining a uniform distribution of beads was more important. The neutrally buoyant beads come in what looks like a powder due to their microscopic size. Their characteristics are well documented by the manufacturer.

3.5. PHANTOM CONSTRUCTION PROCEDURE

To create the ultrasonic phantom specimens, agarose powder is dissolved in water at 90º C. A known concentration of the neutrally buoyant glass bead solution is then added to the mixture and it is shaken until the powder/water mixture has congealed enough to suspend the glass particles throughout. It is possible to speed up the congealing process through the use of cooling in a liquid nitrogen or ice bath, but this must be done with caution as it can sometimes lead to flaws on the surface of the specimen. It also does not work for large specimens.

3.6. PHANTOM CHARACTERIZATION

Because of our unique application it was necessary to determine the scattering characteristics of the phantoms, as no prior literature exists on the specific bead/agarose combination chosen. In order for the half-space approximation to be valid, the amount of acoustic energy emerging from the far side of the phantom was chosen to be approximately 3% of that incident on its face. The phantoms were characterized by measurements of wave speed and attenuation. Because the phantoms are ~98% water, the speed of sound in them was found to deviate little from that in water. Attenuations, however, are found to have a strong dependence on the quantity of beads used in phantom construction.

Figure 17. Phantom construction.

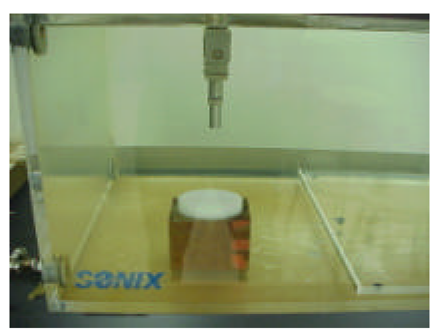

Figure 18. Attenuation measurement set-up.

To investigate the wave speed and attenuation characteristics of the bead/agarose mixture a standard phantom size is used corresponding to the size of a laboratory Pietri dish, approximately 1.5 cm thick and 8.5 cm in diameter (figure 17). Wave speed and attenuation measurements are then performed using a pulse-echo ultrasonic test set-up as shown in figure 18. A theoretical model of the received ultrasonic signal from this experiment can be derived in terms of the attenuation of water, α_w, the attenuation of the phantom, α_p, and the propagation distances L_w and L_p. Without the agarose specimen, the total voltage received at the transducer can be expressed as

$$\overline{V}(t) = R_{Al} V_o e^{-2a_w(L_w + L_p)}, \tag{19}$$

where R_{Al} is the water/aluminum reflection coefficient. When the specimen is replaced, the total received voltage is reduced, and expressed as

$$V(t) = R_{Al} T_p{}^2 V_o e^{-2(a_w L_w + a_p L_p)}. \tag{20}$$

Now divide the reduced voltage by the total voltage, giving

$$\frac{V(t)}{\overline{V}(t)} = T_p{}^2 e^{-2L_p(a_p - a_w)}, \tag{21}$$

where T_p is the water/phantom transmission coefficient. Since agarose is almost entirely water, T_p can be assumed to be close to one. If the attenuation coefficient of water is also ignored, then equation (21) becomes

$$\frac{V(t)}{\overline{V}(t)} = e^{-2a_p L_p}. \tag{22}$$

This accounts for the attenuation over one round trip from the source to the aluminum and back. If only 3% through transmission is desired through a phantom 7 cm thick, the

size of one of the phantom molds, then the exponent of two in equation (22) drops out, and

$$\frac{V(t)}{\overline{V}(t)} = 0.01 = e^{-0.07a_p}, \tag{23}$$

which gives $a_p = 0.658$ dB/cm. An experiment was run to measure the attenuation as a function of the mass of beads in the phantom. From a regression of the data, it was predicted that

$$a_p(m) = 0.0742m + 0.00890, \tag{24}$$

where m is the mass of beads in the phantom. This allows for the bead mass per 200 mL of water to be calculated. From this equation, substituting in an attenuation of $a_p = 0.658$, we obtain m= 8.75g.

A specimen was created using 9g of beads. This actual specimen was expected to have approximately 3% of the incident energy emerging from the far side. For the test phantom, the actual attenuation was 0.507 dB/cm, which translates to only 2.8% of the incident energy emerging from the far side. This then means that the half-space approximation is valid for a phantom with a bead mass of 9g of beads per 200 mL water.

4.0 DATA COLLECTION AND REDUCTION

Due to a low signal-to-noise ratio the data for the experiment were collected in a manner somewhat different than what was proposed. Low signal strength made it very difficult to observe the incoherent backscatter from the specimen. One significant source of noise identified came from the servo motors for the Sonix C-Scan system. When the C-Scan system was turned off noise reduced significantly but still no backscatter signal

was observable at any of the azimuthal positions. Ultimately, a second noise source was discovered when a malfunctioning preamplifier was identified.

Because the G-Scan motors introduced so much noise, the source transducer could not be moved over the face of the specimen as required for the simulation of a plane. Instead, the source was pulsed at a single point in the phantom, the focal point of the receiver, and backscatter data were collected over eleven azimuthal angles around the specimen. The intensity as a function of time was stored in a file for each of the azimuthal locations. All twelve locations could not be used because the source location was blocked by the C-Scan manipulator.

In order to reduce the data, the intensity files for each location were imported into a Matlab program. A cosine azimuthal decomposition of the backscattered intensity was performed for the first four Legendre coefficients.

4.1. DATA COLLECTION

Before any backscatter data could be taken, it was necessary to focus both the source and the receiver on the same point in space. A 1.5” diameter ball bearing was placed at the center of the stage. Each transducer was adjusted while in pulse-echo mode until the received voltage was maximized. In pulse-echo mode, the transducer acts as a source, and then that same transducer, once it has pulsed, becomes the receiver. When the backscattered voltage off the face of the ball bearing was at a maximum, it was known that the transducer was focused on a point running through the center of the sphere. Both transducers were focused using this method.

It was originally planned to automate the movement of the source over the phantom using the Sonix C-Scan system. However, because of electronic noise generated by the servo motors the source was operated through a Panametrics Computer-Controlled Pulser/Receiver. The output from this was then sent into one of the input channels of a Lecroy 9350CM 500Mhz Oscilloscope. The receiver was run through a Panametrics ultrasonic preamplifier and then into the other channel of the oscilloscope. When the servo motors were turned on to begin the traversal, the backscattered signal at the receiver became lost in the noise. As a result of the significant noise, it was determined that the experiment could not be automated using the Sonix C-scan system.

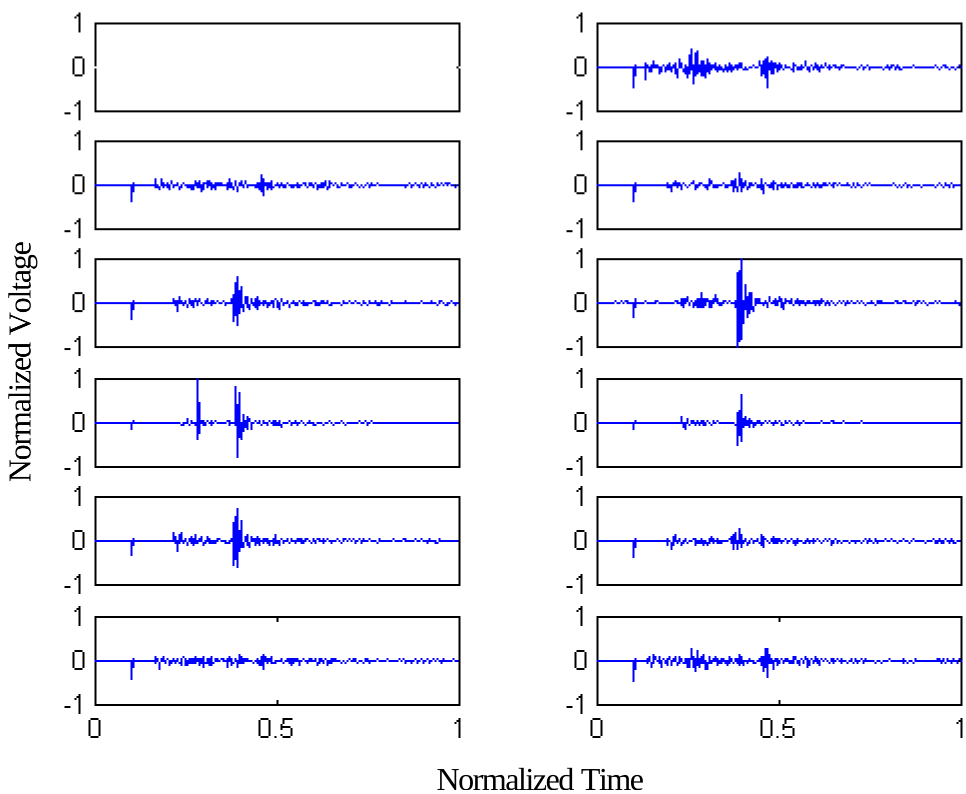

Figure 19. Backscattered intensity received at each azimuthal position.

In order to obtain some data, the source and receiver were focused at a single point in the phantom as previously described. The backscattered intensity was then measured at the twelve available azimuthal positions (figure 19). One position was unavailable due to the source transducer being an obstruction and is represented as the first graph with no data. At each azimuthal position, the backscattered intensity at the receiver was averaged over 100 source pulses. This was done with the averaging function on the oscilloscope.

Figure (20) shows a plot of the backscattered intensity received at one of the azimuthal positions. The first large spike is a result of the pulse of the transducer. What follows the initial large spike is the diffuse backscattered intensity. Figure (21) represents all the backscatter data received at each of the azimuthal angles, with time extending along the radial lines. The layout gives an idea of the contribution coming from each direction. The data from each position was then saved into a data file for reduction in Matlab.

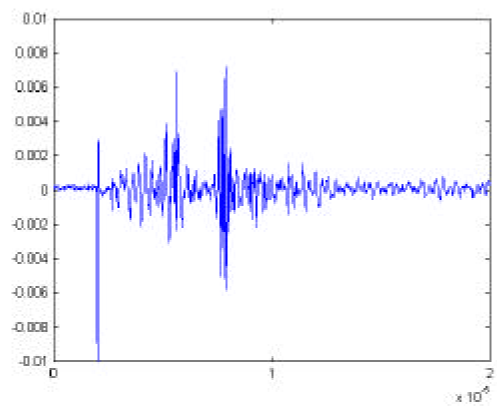

Figure 20. Received backscatter signal at one azimuthal position.

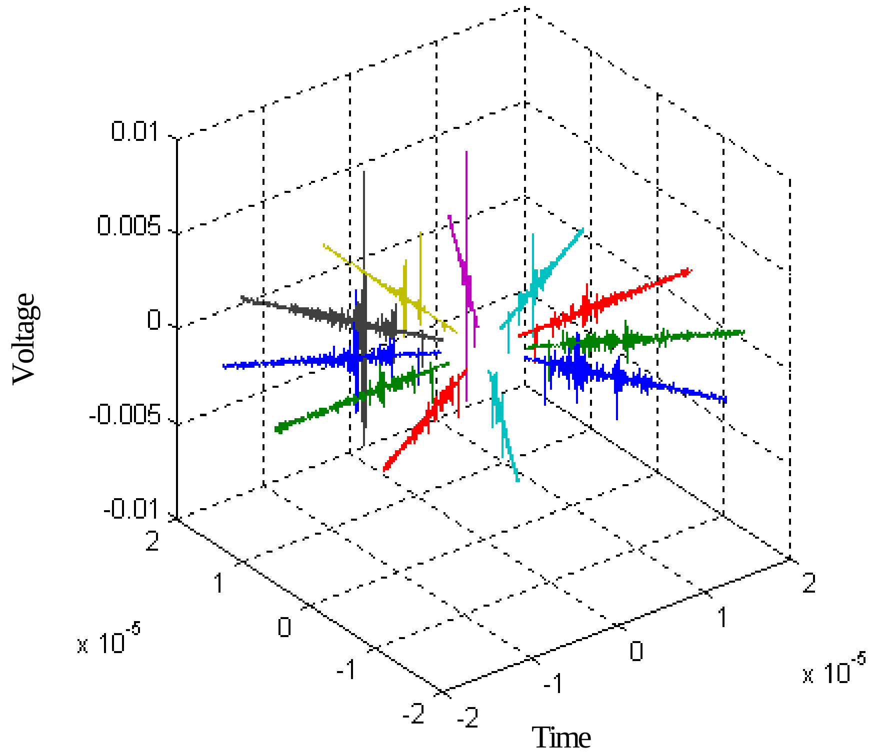

Figure 21. Backscattered intensity at each of the eleven azimuthal positions.

4.2. DATA REDUCTION

The goal of the data reduction method is to produce the Fourier azimuthal moments, $I^m(m,t)$, of the backscatter intensity. The data obtained from the experiment have the backscattered intensity, $I(0,m_s,j,t)$, at the surface of the specimen, z=0, at the fixed polar angle of the source, m_s, and as a function of azimuthal angle and time. Figure (22) helps to visualize the data.

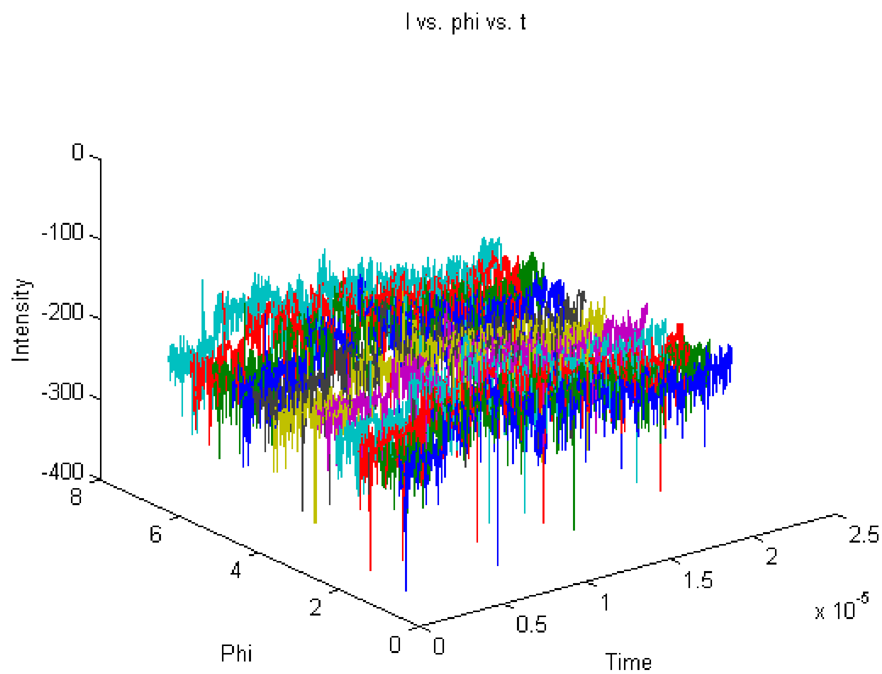

Figure 22. Backscattered intensity as a function of azimuthal angle and time.

The Fourier azimuthal moments, I^m, can now be calculated, using their definition in equation (17), by taking the Fourier cosine decomposition of $I(0, m_s, j, t)$ in the f direction at fixed times. The results of this decomposition for the first four moments, m=0,1,2,3, are shown in figure (23). The individual azimuthal moments as a function of

time are shown again in figure (24) for clarity.

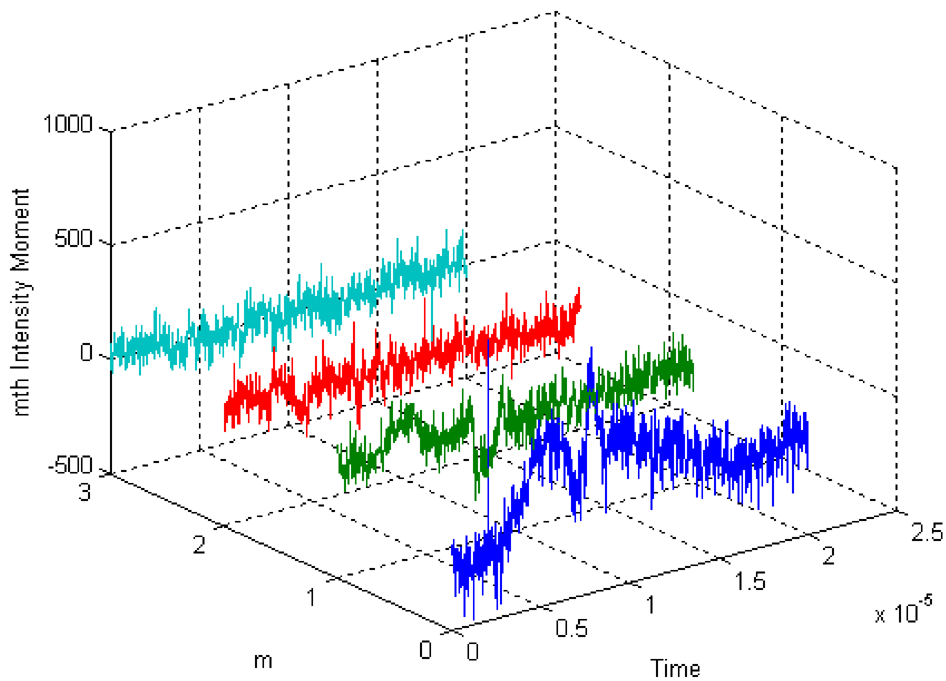

Figure 23. Azimuthal moments of intensity, I^0, I^1, I^2 ,I^3.

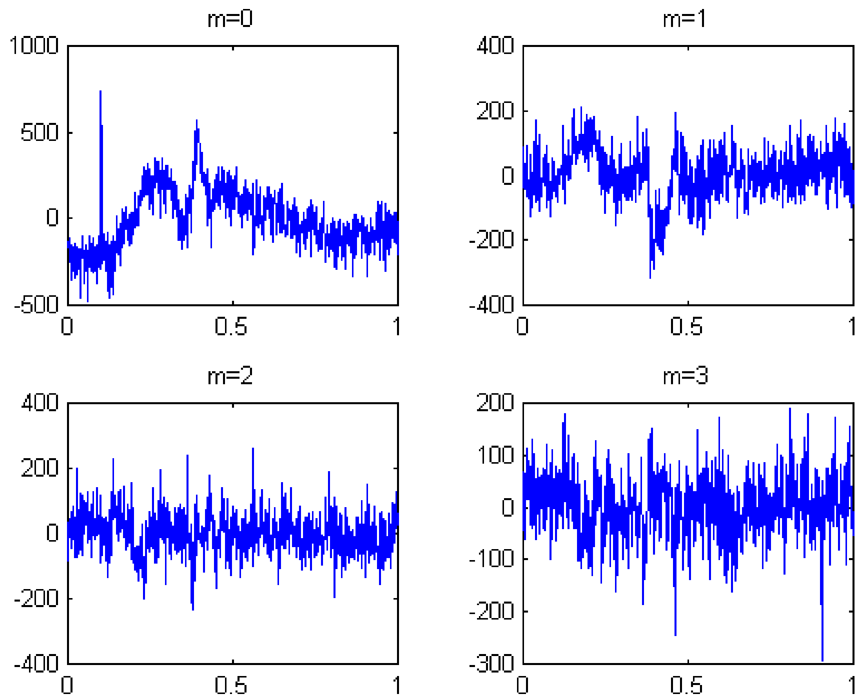

Figure 24. Azimuthal moments of intensity, I^0, I^1, I^2 ,I^3.

4.3. INVERSE PARAMETER DETERMINATION

In order to obtain the Legendre weighting factors, Matlab was used to do a nonlinear fit to the azimuthal moments of intensity obtained in section 4.2. Due to the noise, only the zeroth weighting factor could be approximated. A value of approximately one was expected. The obtained value was many orders of magnitude larger, once again, as a result of the noise and the fact that only a point scan was done.

5.0 CONCLUSION

The accuracy of the inverse method under investigation was not determined due to delays in the acquisition of the backscattered intensity from the phantom. Acquisition of these data was significantly delayed because of signal to noise ratio problems in the data acquisition system as a result of the operation of the C-Scan system and the presence of a malfunctioning preamplifier.

Replacing the malfunctioning preamplifier and not using the C-Scan system during data acquisition solved the problems with data acquisition noise. The loss of the C-Scan system during data acquisition causes significant complications, however. The plane wave superposition solution planned for the experiment could not be accomplished in an automated fashion. The scan pattern must now be performed by hand. This has significantly delayed the acquisition of backscattered intensities for a simulated plane wave source. Acquisition of these data using a hand scan will be completed as future work, but is very tedious and time intensive.

Despite the setbacks in data acquisition, a variety of significant accomplishments were made. Just setting up a data acquisition system was quite significant, as nothing of that nature has ever been done for ultrasonics. Also, suitable phantoms that could be used in the devised acquisition scheme were generated. Finally, a robust experimental apparatus that interfaced well with the Sonix C-Scan to facilitate data acquisition was also successfully built.

Appendix (1): Characteristics for transducers from frequencies of 0.5 to 10Mhz

Large Diameter Case Style

Freq	Diam (in)	Focal Length (in)	Near Field (in)	Norm. Focal lgth (in)	Beam Diameter (in.)	Focal Zone	Beam Width (in.)
5.00E+05	1.500	2.150	4.757	0.452	0.1741	1.585	5.4660
5.00E+05	1.125	1.500	2.661	0.564	0.1629	1.319	7.2966
5.00E+05	1.000	1.250	2.095	0.597	0.1532	1.149	8.2146
5.00E+05	0.750	0.780	1.164	0.670	0.1291	0.783	10.9825
1.00E+06	1.500	2.500	9.559	0.262	0.1007	1.156	2.7299
1.00E+06	1.125	1.900	5.366	0.354	0.1023	1.143	3.6409
1.00E+06	1.000	1.625	4.235	0.384	0.0985	1.046	4.0968
1.00E+06	0.750	1.000	2.372	0.422	0.0812	0.696	5.4660
2.25E+06	1.500	2.700	21.534	0.125	0.0483	0.637	1.2129
2.25E+06	1.125	2.150	12.099	0.178	0.0513	0.702	1.6173
2.25E+06	1.000	1.875	9.554	0.196	0.0504	0.670	1.8195
2.25E+06	0.750	1.000	5.364	0.186	0.0359	0.341	2.4264
3.50E+06	1.000	1.950	14.868	0.131	0.0337	0.480	1.1696
3.50E+06	0.750	1.000	8.350	0.120	0.0231	0.226	1.5595
5.00E+06	1.000	1.950	21.243	0.092	0.0236	0.342	0.8187
5.00E+06	0.750	1.000	11.932	0.084	0.0161	0.161	1.0916
7.50E+06	0.750	1.000	17.900	0.056	0.0108	0.109	0.7277
1.00E+07	1.000	2.000	42.490	0.047	0.0121	0.184	0.4093
1.00E+07	0.750	1.000	23.868	0.042	0.0081	0.082	0.5458

Standard Case Style

Freq	Diam (in)	Focal Length (in)	Near Field (in)	Norm. Focal lgth (in)	Beam Diameter (in.)	Focal Zone	Beam Width (in.)
1.00E+06	0.500	0.600	1.043	0.575	0.0739	0.536	8.2146
2.25E+06	0.5	0.800	2.374	0.337	0.0433	0.461	3.6409
2.25E+06	0.375	0.500	1.329	0.376	0.0362	0.317	4.8571
2.25E+06	0.25	0.350	0.584	0.599	0.0385	0.323	7.2966
3.50E+06	0.5	0.830	3.699	0.224	0.0288	0.335	2.3397
3.50E+06	0.375	0.600	2.073	0.289	0.0279	0.303	3.1202
3.50E+06	0.25	0.385	0.914	0.421	0.0270	0.268	4.6832
5.00E+06	0.5	0.750	5.287	0.142	0.0182	0.199	1.6375
5.00E+06	0.375	0.600	2.965	0.202	0.0195	0.221	2.1836
5.00E+06	0.25	0.430	1.309	0.328	0.0211	0.243	3.2764
7.50E+06	0.5	0.750	7.933	0.095	0.0121	0.135	1.0916
1.00E+07	0.5	0.750	10.579	0.071	0.0091	0.103	0.8187
1.00E+07	0.375	0.600	5.934	0.101	0.0097	0.115	1.0916
1.00E+07	0.25	0.460	2.622	0.175	0.0113	0.148	1.6375
1.50E+07	0.5	0.750	15.870	0.047	0.0061	0.069	0.5458
1.50E+07	0.375	0.600	8.902	0.067	0.0065	0.078	0.7277
1.50E+07	0.25	0.500	3.935	0.127	0.0082	0.119	1.0916
2.00E+07	0.25	0.500	5.247	0.095	0.0061	0.091	0.8187
2.00E+07	0.125	0.250	1.290	0.194	0.0062	0.088	1.6375

Works Cited

American Society for Nondestructive Testing, *Nondestructive Testing Handbook, 2^{nd} Edition* (Columbus, 1982).

Barabanenkov, Y. N. and V. M. Finkel’berg, “Radiation transport equation for correlated scatterers,” *Zh. Eksp. Fiz.* **53**, 978-986 (1967) [*Soviet Physics – JETP* **26**, 587-591 (1968)].

Boyce, W. E., and R. C. DiPrima, *Elementary Differential Equations and Boundary Value Problems* (Wiley, New York, 1977).

Bridal, S. L., K. D. Wallace, R. L. Trousil, S. A. Wickline, and J. G. Miller, “Frequency dependence of acoustic backscatter from 5 to 65 MHz (0.06<ka<4.0) of polystyrene beads in agarose,” *Journal of the Acoustical Society of America* **100**, 1841-1848 (1996).

Burlew, M. M, E. L. Madsen, J. A. Zagzebski, R. A. Banjavic, and S. W. Sum, "A new ultrasound tissue-equivelent material," *Radiology*, **134**, 517-520 (1980).

Chandrasekhar, S., *Radiative Transfer* (Dover, New York, 1960).

Elliot, R. A., T. Duracz, N. J. McCormick, and D. R. Emmons, “Experimental test of a time-dependant inverse radiative transfer algorithm for estimating scattering parameters,” *Journal of the Optical Society of America* **5**, 366-373 (1988).

Elliot, R. A., T. Duracz, N. J. McCormick, and D. R. Emmons, “Experimental test of a time-dependant inverse radiative transfer algorithm for estimating scattering parameters:addendum,” *Journal of the Optical Society of America* **6**, 603-606 (1989).

Ishimaru, A., *Wave Propagation and Scattering in Random Media* (Academic Press, New York, 1978).

Kinsler, L. E., A. R. Frey, A. B. Coppens, and J. V. Sanders, *Fundamentals of Acoustics* (Wiley, New York, 1982).

Kreyszig, E., *Advanced Engineering Mathematics* (Wiley, New York, 1993).

McCormick, N. J., "Remote characterization of a thick slab target with a pulsed laser," *Journal of the Optical Society of America* **6**, 756-759 (1982).

Turner, J. A., "Radiative Transfer of Ultrasound," Diss., University of Illinois at Urbana Champaign, 1994.

Valéry, R., S. L. Bridal, P. Laugier, and G. Berger, "Absolute Backscatter Coefficient over a Wide Range of Frequencies in a Tissue-Mimicking Phantom Containing Two Populations of Scatterers," *IEEE Transactions on Ultrasonics, and Frequency Control* **43**, 970-978 (1996).

Weaver, R. L., "Diffusivity of ultrasound in polycrystals," *Journal of the Mechanics and Physics of Solids* **38**, 55-86 (1990).

Weaver, R. L., "On diffuse waves in solid media," *Journal of the Acoustica Society of America* **71**, 1608-1609 (1982).

Weaver, R. L., W. Sachse, K. Green, and Y. Zhang, "Diffuse ultrasound in polycrystalline solids," Proceedings of Ultrasonics International, Le Touquet, France, July, 1991.